Journal of Alloys and Compounds 506 (2010) 640–644

Contents lists available at ScienceDirect

Journal of Alloys and Compounds

journal homepage: www.elsevier.com/locate/jallcom

Compressibility and sinterability of Al_2O_3–YAG nanocomposite powder synthesized by an aqueous sol–gel method

S.A. Hassanzadeh-Tabrizi [a], E. Taheri-Nassaj [b,*]

[a] Department of Materials Engineering, Islamic Azad University, Najafabad Branch, Isfahan, Iran
[b] Department of Materials Science and Engineering, Tarbiat Modares University, PO Box 14115-143, Tehran, Iran

ARTICLE INFO

Article history:
Received 3 September 2009
Received in revised form 5 July 2010
Accepted 7 July 2010
Available online 15 July 2010

Keywords:
Ceramic–matrix nanocomposites
Compaction
Sintering
Electron microscopy

ABSTRACT

In the present work, the compressibility and sinterability of Al_2O_3–YAG nanocomposite powder prepared by an aqueous sol–gel method have been investigated. An amorphous nanopowder was synthesized, and it was crystallized to Al_2O_3–YAG, with an average particle crystallite size of 50 nm, after heat-treatment via a solid-state reaction. It was shown that the compressibility curve of this powder is characterized by two linear parts at low and middle pressures. The agglomeration strength of the powder was about 142 MPa. The densification of composites started at 1000 °C. The relative density and grain size of sintered Al_2O_3–0.75 mol Y_2O_3 were measured to be 96% and 650 nm at 1500 °C, respectively. TEM results showed a sub-micronic/nano microstructure is formed. The amount of Y_2O_3 had a strong effect on the sintering behavior and final microstructure of nanocomposite powders and it inhibited alumina grain growth and suppressed densification process.

1. Introduction

Alumina is an important ceramic material in industrial applications [1,2]. The creep behavior and mechanical properties of alumina ceramics can be improved by dispersing YAG ($Y_3Al_5O_{12}$, yttrium aluminum garnet) particles in alumina matrix [3–5]. Therefore, the Al_2O_3–YAG composite has received much attention in high temperature applications.

The sintering behavior and the evolution of the microstructure of ceramics are significantly affected by the ceramic processing including the initial powder state, forming additives, and sintering processes. It has been reported that the synthesis method has an obvious influence on the powder characteristics. In other words, powders synthesized by different methods have different sintering behavior [6–9]. More recently, the synthesized ultra fine powders with particle size less than 100 nm have provided new opportunities. A great deal of research has been made on such materials because of the promise of new and interesting properties. Nanopowders have significantly enhanced sintering rates and decreased sintering temperatures compared to micrometer-sized particles due to higher surface area [10–13].

Sol–gel method is an attractive synthetic route for the preparation of nano-sized inorganic powders with homogeneous mixture of the several components at a molecular level [14,15]. In addition, it provides powders with low sintering temperatures and uniform particle sizes [16]. Recently new and economical procedures have been developed for synthesis of nano alumina using Al powder and $AlCl_3$ [2,17]. In the present work, Al_2O_3–YAG nanocomposite powder was synthesized using the same raw materials in their works and Y_2O_3 through a sol–gel method. The compressibility and sinterability of this nanopowder were investigated in detail.

2. Experimental procedure

Al_2O_3–YAG composite powder was prepared by a sol–gel method using $AlCl_3{\cdot}6H_2O$ (Merck), Al powder with d_{50} = 37.5 μm (M. A. University), Y_2O_3 (Sigma–Aldrich) and HCl (Merck). First Y_2O_3 was dissolved in aqueous HCl. The main solution was prepared by dissolving $AlCl_3{\cdot}6H_2O$, Al powder and Y_2O_3 solution into the deionized water. The amounts of yttria in composite samples were 0.75, 1.5 and 3 mol%. One specimen was prepared by the same processing, without using yttrium oxide powder (pure alumina). The molar ratios of $Al/AlCl_3$ and HCl/H_2O were 2 and 0.18, respectively. The precursor solution was stirred at 100 °C for 4 h and was aged at 60 °C until the batch set to a rigid gel. It was then dried at 80 °C for 48 h. The resultant synthesis product (gel) has been calcined at 800 °C for 30 min to remove water and volatile components. In order to reduce the amount of hard agglomerates, the calcined nanopowder was wet-planetary milled using a high dense alumina jar and high pure alumina balls for 1 h. The powders with different Y_2O_3 contents were pressed into compacts, using a uniaxial press at the pressure of 300 MPa. The compacts were then sintered in a tube furnace under air atmosphere at various temperatures for 3 h with a heating rate of 6 °C/min.

The crystalline structure of the powders and composite samples were determined by X-ray diffraction using Philips X-pert model with Cu Kα radiation. The average crystallite size of the powder was estimated from the Scherrer equation. The densities of the sintered specimens were measured by the Archimedes method, which gave reproducible results to within ±0.2%. The microstructures of powders and sintered specimens were observed by scanning electron microscopy (SEM, XL30-Phillips) and transmission electron microscopy (TEM, CM200-FEG-Phillips).

* Corresponding author. Tel.: +98 21 82883306; fax: +98 21 88005040.
E-mail address: taheri@modares.ac.ir (E. Taheri-Nassaj).

0925-8388/$ – see front matter © 2010 Elsevier B.V. All rights reserved.
doi:10.1016/j.jallcom.2010.07.030

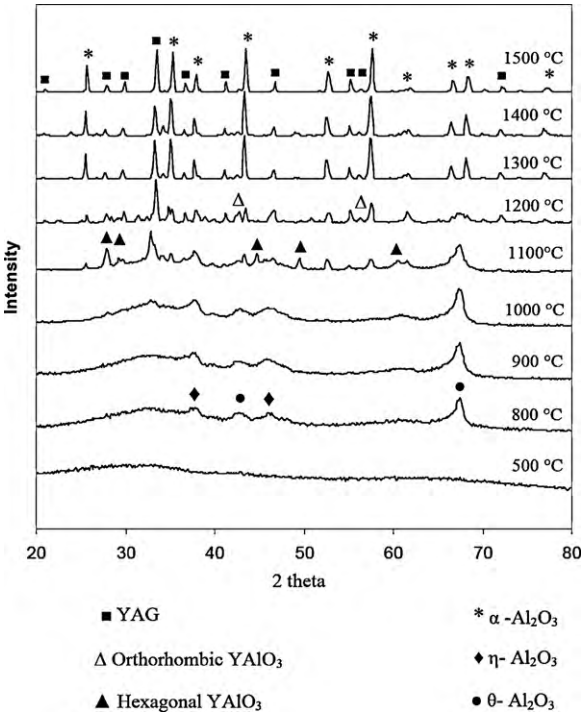

Fig. 1. The XRD patterns of an Al_2O_3–1.5 mol% Y_2O_3 nanocomposite powder calcined at different temperatures.

Also, energy-dispersive X-ray spectroscopy (EDS) was conducted using TEM for chemical analysis of the grains.

3. Results and discussion

The synthesis mechanism may be described by the following reactions. Yttrium oxide first reacts with HCl and forms yttrium chloride (reaction (1)).

$$Y_2O_3 + 6HCl \Leftrightarrow 2YCl_3 + 3H_2O \quad (1)$$

Then aluminum chloride hexahydrate and yttrium chloride may be hydrolyzed to produce the sol (reactions (2) and (3)).

$$AlCl_3 + 3H_2O \Leftrightarrow Al(OH)_3 + 3HCl \quad (2)$$

$$YCl_3 + 3H_2O \Leftrightarrow Y(OH)_3 + 3HCl \quad (3)$$

Reaction (4) shows that Al powder reacts with HCl to produce aluminum chloride and hydrogen gas and therefore Al can be used as a source of $AlCl_3$.

$$2Al + 6HCl \Leftrightarrow 2AlCl_3 + 3H_2 \quad (4)$$

Finally, the hydroxides groups produced in reactions (2) and (3) aggregate together to form the gel.

Fig. 1 shows the XRD patterns of an Al_2O_3–1.5 mol% Y_2O_3 nanocomposite powder calcined at different temperatures. As can be seen the powder heat-treated at 500 °C does not have any peaks and seems to be amorphous. By increasing the heat-treatment temperature to 800 °C, the powder is crystallized to θ-Al_2O_3 and η-Al_2O_3 phases. The specimens with different amounts of Y_2O_3 contained the same phases after heat-treatment at 500 and 800 °C. The average crystallite size of powders was determined by means of the X-ray line-broadening method to be 45 nm at 800 °C. By increasing the temperature some transition phase of YAG (hexagonal $YAlO_3$, YAP) are formed. However, at higher temperatures α-Al_2O_3 and YAG are appeared in all composite specimens.

Fig. 2 illustrates TEM micrographs of powder heat-treated at 800 °C and milling for 1 h. As can be seen in Fig. 2(a) some agglomerations exist in the powders which are attributed to uncontrolled coagulation during gelation and the formation of necks during calcination. Fig. 2(b) shows the nanoparticles. The grain size of the powders is about 45–50 nm which is in agreement with the Scherrer equation results.

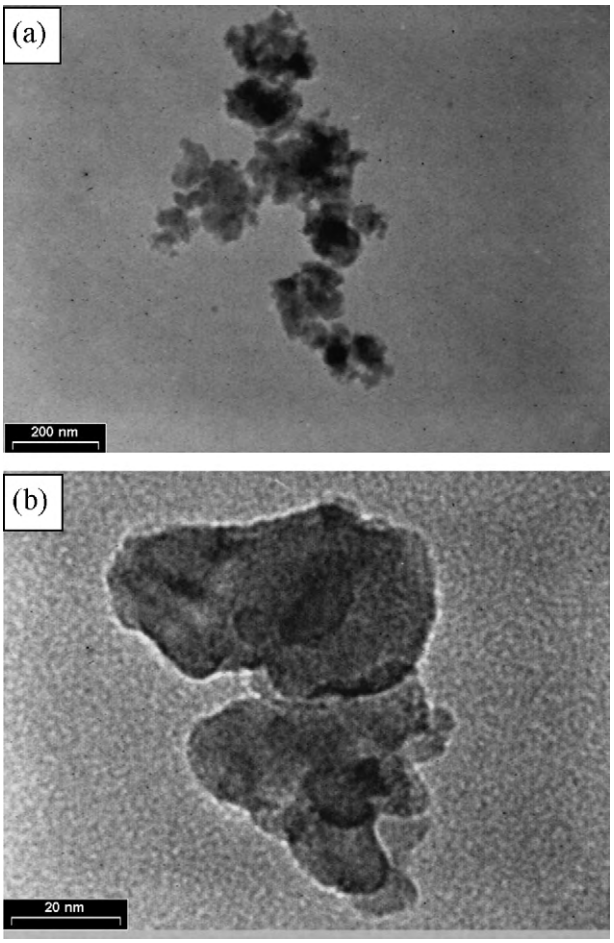

Fig. 2. TEM micrographs of powders heat-treated at 800 °C and milling for 1 h (a) agglomerates (b) nanoparticles.

One of the most crucial features for producing dense ceramics is the powder compressibility, by which the compact green density and therefore the fired density are directly contributed. It is known that the compaction mechanism of brittle powders in a rigid die is usually considered in three stages including; (I) sliding and rearrangement of the particles; (II) fragmentation of brittle solids and (III) elastic deformation of bulk compacted powders [7]. At the first stage of the compaction process, particle sliding and rearrangement of the agglomerates particles are the dominant mechanisms of consolidation. When the applied pressure increases, the movement of the particles is restricted and the energy applied to the powder compact is spent generally through the process of fragmentation of agglomerates and friction losses. Groot Zevert et al. [18] showed that in the case of the agglomerated powders, there was a turning point (P_y) in the plot of the relative density versus logarithm of the applied pressure, like that shown in Fig. 3. The curve was divided into two sharply separated linear parts with an interception at point P_y. The interception was called "strength of the agglomerates". After compaction at a pressure of around P_y, these agglomerates were gradually fragmented and then rearranged at lower pressures [18]. As can be seen the agglomeration strength of the powder is about 142 MPa. The value of P_y depends heavily on the method of synthesis and calcination temperature [19].

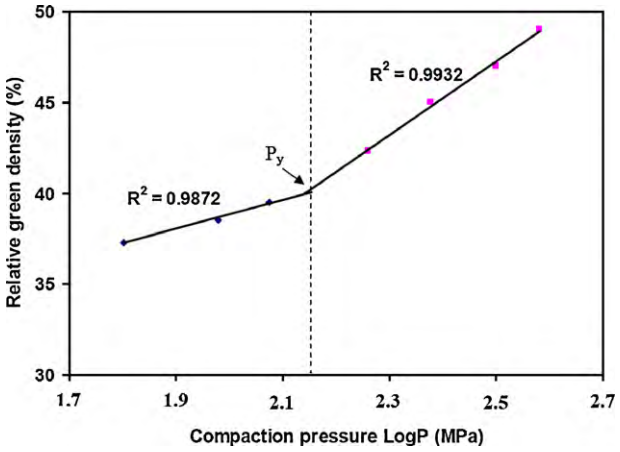

Fig. 3. Relative green densities of composite nanopowder as function of log compaction pressure (*P*).

Fig. 4 shows the changes of the fractional density and grain size versus the fired temperature of Al_2O_3–0.75 mol% Y_2O_3. The density versus temperature plot exhibited a sigmoidal shape. As seen, the sintering rate below 1300 °C was slow. The rate of densification increased drastically at 1350 °C and a significant densification was obtained at about 1450 °C. As a consequence, the increase of temperature from 1350 to 1450 °C increased the fractional density from 70 to 92.5 of theoretical density. With further increasing of the sintering temperature, a relatively slight increase was obtained in the density. The change of grain size as a function of sintering temperature presents two distinct regions. At the first region, between 1200 and 1400 °C, the rate of grain growth was slow in which the grain size increased from 51 to 199 nm. In the second stage of sintering (usually between 0.65 and 0.9 theoretical density), according to the solid-state sintering mechanism, dispersed open pores could pin grain boundaries and hinder grain boundary migration, for which the grain growth was suppressed. Second region was related to temperatures higher than 1400 °C. In this region, the final grain size of the sintered samples was sharply increased. It shows a significant grain growth at the final stage of sintering happening at 1500 °C. It was confirmed that the open pores (referring to the intermediate stage of sintering) collapsed to form closed pores, after which the final stage of sintering started. Such a collapse resulted in a substantial decrease in pore pinning, which triggers the accelerated grain growth. One reason for limitation of density (96%) is due to dry-pressing process. As it is known, by uniaxial pressing the external force can never arrive on an individual particle in the body to shift it into an optimum position between its neighbors. Therefore, this

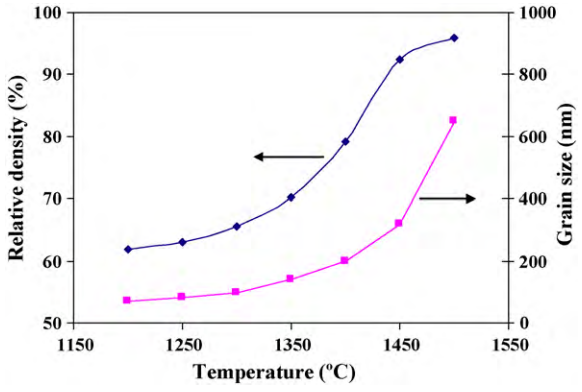

Fig. 4. Density and grain size of sintered Al_2O_3–0.75 mol% Y_2O_3 nanocomposite powder as a function of sintering temperature.

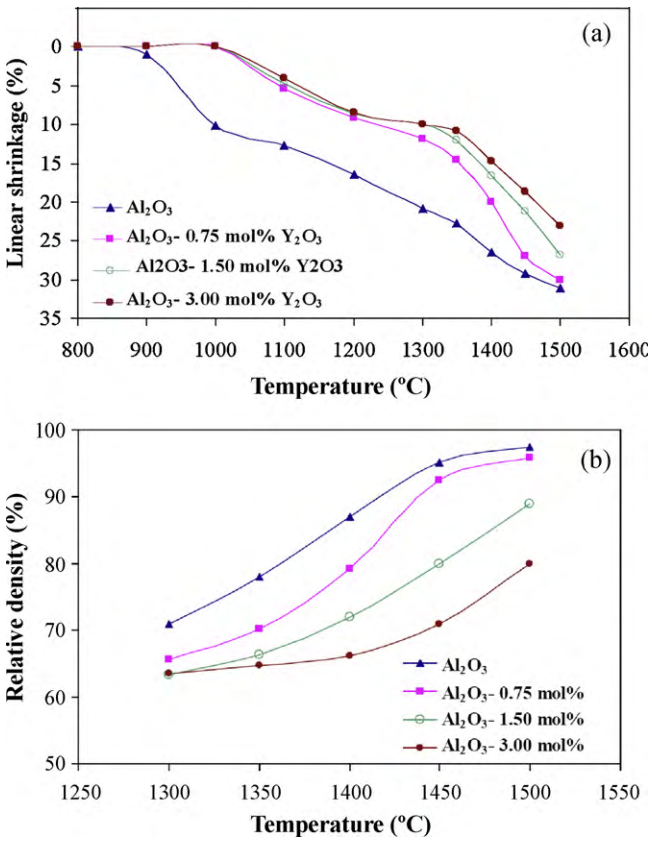

Fig. 5. (a) Linear shrinkage and (b) relative density of samples with different Y_2O_3 contents as a function of sintering temperature.

method generates a tail of large pores. According to a sintering law modified by Mayo [20] the highest densification rate occurs for the finest pore size. Therefore, pores smaller than the critical size will shrink, while larger pores undergo the pore-boundary separation and remain. It reduces the density in all sintered specimens.

Fig. 5 shows linear shrinkage and relative density of samples with different Y_2O_3 content as a function of sintering temperature. As can be seen in Fig. 5(a) all composite materials presented different sintering behaviors compared to the pure alumina. Alumina began to shrink at around 900 °C, whereas composite samples started to densify at around 1000 °C. According to these results, it is clear that the addition of yttria increases the starting point of sintering of the alumina. It seems that, this effect is related to the yttrium segregation in the grain boundaries. Segregation of Y to grain boundaries arises from a large size mismatch between Al^{3+} (0.051 nm) and Y^{3+} (0.089 nm) radius. In addition the shrinkage of sintered composite specimens decreased with increasing the amount of Y_2O_3 at temperatures higher than 1200 °C. This may be attributed to the formation of YAP (yttrium aluminum perovskite, $YAlO_3$) and YAG phases (Fig. 1).

Fig. 5(b) depicts the relative density of the samples with different Y_2O_3 content versus the sintering temperature. The relative density was 97.2% for pure alumina sintered at 1500 °C for 3 h, whereas a relative density of 96% was attained for 0.75 mol% Y_2O_3 doped sample under the same sintering conditions. Relatively lower densities were obtained for the samples doped with 1.5 and 3 mol% Y_2O_3, respectively. Therefore, it seems that the sintering of these composites needs higher sintering temperatures (above 1500 °C). For Instance, Duong et al. could obtain a relative density of 98% after sintering alumina–50% YAG and alumina–75% YAG composites at high temperature of 1600 °C for 120 h [21].

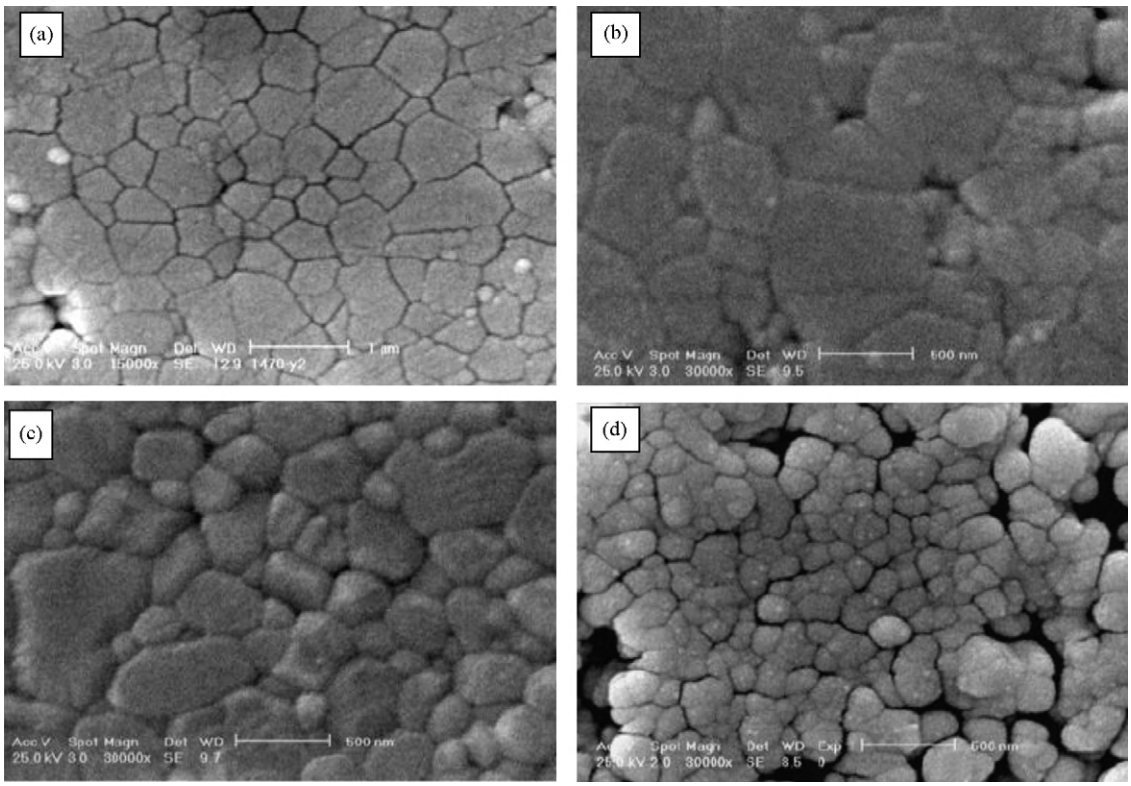

Fig. 6. Scanning electron micrographs of specimens sintered at 1500 °C for 3 h with (a) 0, (b) 0.75, (c) 1.5 and (d) 3 mol% of Y_2O_3, respectively.

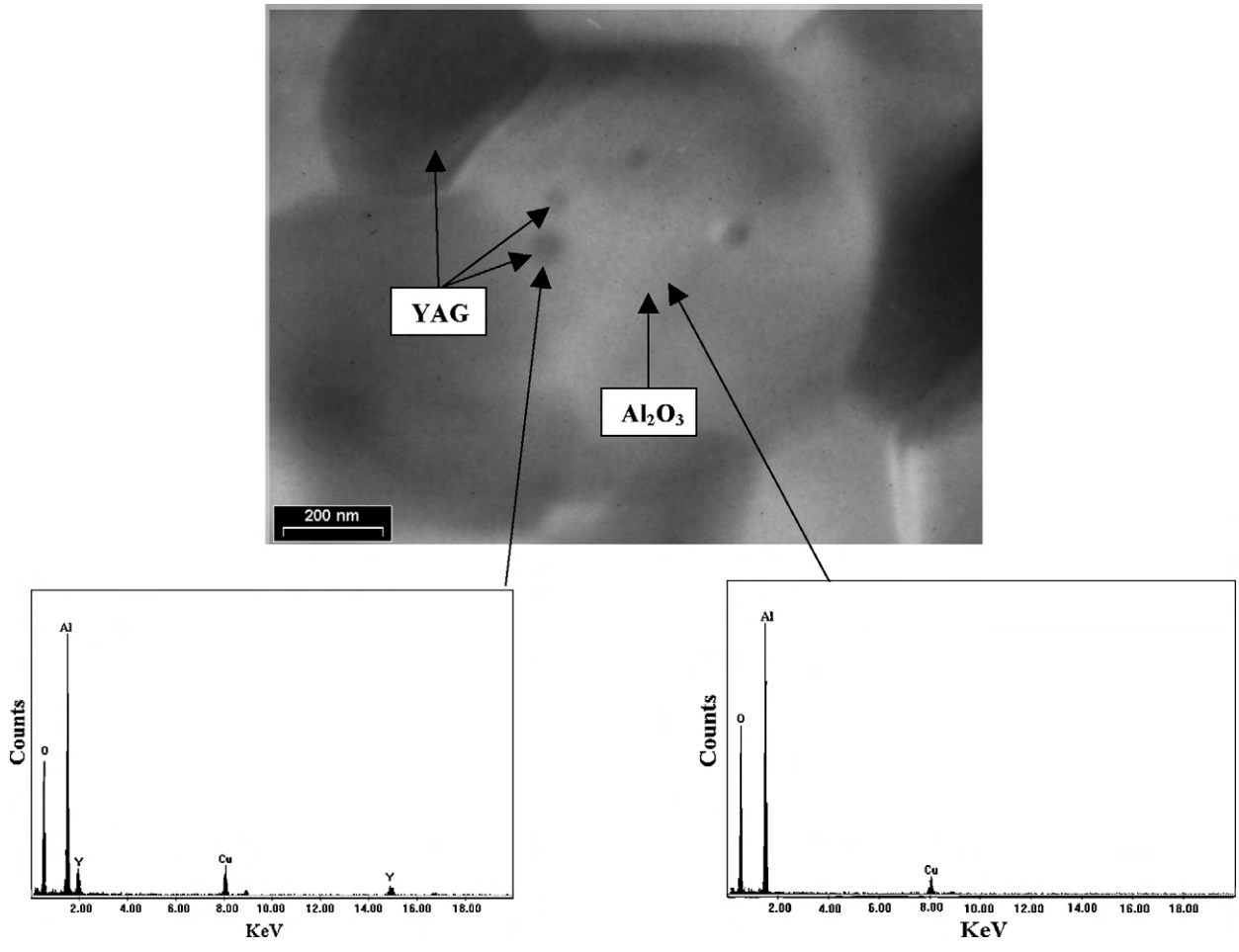

Fig. 7. TEM micrograph and EDS analyses of Al_2O_3–0.75 mol% Y_2O_3 composite sintered at 1500 °C.

The microstructures of the samples after sintering at 1500 °C for 3 h are shown in Fig. 6(a–d). Microstructural observation showed that grain growth occurs in pure alumina at 1500 °C. As can be seen, an inhomogeneous equiaxed microstructure with a mean grain size of about 1 μm is observed. The composite samples with 0.75, 1.5 and 3 mol% Y_2O_3 additives, have microstructures with the mean grain size of about 650, 350 and less than 200 nm, respectively. Intergranular pores are clearly visible in the microstructure of 3 mol% Y_2O_3 sample. It can be seen that the presence of yttria inhibits alumina grain growth and suppresses densification process. This may be because when pure alumina is doped over the solubility limit with Y^{3+}, a pinning effect takes place at grain boundaries due to the formation of YAP and YAG phases. The pinning process blocks grain boundary during sintering [1]. In addition, it was shown that the powder calcined at 800 °C contained the metastable phases of Al_2O_3, θ and η-Al_2O_3, which were transformed to stable α-Al_2O_3 after sintering (see Fig. 1). These transformations are associated with pore formation due to density differences between the phases and the final sintering stage of alumina takes place after these transformations. It was reported that the presence of yttria postpones the formation of α-alumina [14]. Therefore, the sintering temperature shifts to higher temperatures to eliminate the pore networks developed during the transformation when Y_2O_3 is added to alumina.

TEM image and EDS analyses of the Al_2O_3–0.75 mol% Y_2O_3 composite sintered at 1500 °C are shown in Fig. 7. The contrasted dark and bright areas within the images on the nanocomposites correspond to the YAG and Al_2O_3 phases, respectively. Some YAG particles about 500 nm were located between grains while some other spherical YAG nanoparticles about 50 nm were embedded in the Al_2O_3 grains. The corresponding EDS spectrums taken from the bright and dark areas confirm the presence of Al and O in bright areas and Y, Al and O in dark areas. The source of Cu in the EDS spectrums corresponds to the holder used for specimens. Following Niihara's classification [22], these nanocomposites show both intratype/intertype microstructures.

4. Conclusions

In the present study, the compressibility and sinterability of Al_2O_3–YAG nanocomposite powder prepared by an aqueous sol–gel method have been investigated. The findings can be summarized as follow:

(1) The synthesized nanopowders consisted of some agglomerates and some individual nanoparticles after heat-treatment at 800 °C. The grain size of the powders was about 45–50 nm. The compressibility curve was characterized by two linear parts at low and middle pressures. The agglomeration strength of the powder was about 142 MPa.
(2) The relative density and grain size of sintered Al_2O_3–0.75 mol Y_2O_3 were measured to be 96% and 650 nm at 1500 °C, respectively. Densification of pure alumina started at around 900 °C, whereas all composite specimens started to densify at around 1000 °C.
(3) The Y_2O_3 and formed YAG phase in nanocomposite samples inhibited both sintering and grain growth processes.
(4) TEM micrograph revealed that some YAG particles (about 500 nm) are located between grains, whereas some other spherical YAG nanoparticles (about 50 nm) are embedded within Al_2O_3 grains.

References

[1] M. Schel, L.A. Diaz, R. Torrecillas, Acta Mater. 50 (2002) 1125–1139.
[2] S.A. Hassanzadeh-Tabrizi, E. Taheri-Nassaj, Mater. Lett. 63 (2009) 2274–2276.
[3] J. Cho, M.P. Harmer, H.M. Chan, J.M. Rickman, A.M. Thompson, J. Am. Ceram. Soc. 80 (1997) 1013–1017.
[4] R. Torrecillas, M. Schehl, L.A. Diaz, J.L. Menendes, J.S. Moya, J. Eur. Ceram. Soc. 27 (2007) 143–150.
[5] W.Q. Li, L. Gao, Nanostruct. Mater. 11 (1999) 1073–1080.
[6] F.S. Shiau, T.T. Fang, T.H. Leu, Mater. Chem. Phys. 57 (1998) 33–40.
[7] P. Bowen, C. Carry, Powder Technol. 128 (2002) 248–255.
[8] W. Li, L. Gao, Scripta Mater. 44 (2001) 2269–2272.
[9] L. Stanciu, J.R. Groza, L. Stoica, C. Plapcianu, Scripta Mater. 50 (2004) 1259–1262.
[10] S.C. Tjong, H. Chen, Mater. Sci. Eng. R 45 (2004) 1–88.
[11] M.J. Iqbal, M.N. Ashiq, Scripta Mater. 56 (2007) 145–148.
[12] J. Markmann, A. Tschope, R. Birringer, Acta Mater. 50 (2002) 1433–1440.
[13] P. Palmero, A. Simone, C. Esnouf, G. Fantozzi, L. Montanaro, J. Eur. Ceram. Soc. 26 (2005) 941–947.
[14] S.A. Hassanzadeh-Tabrizi, E. Taheri-Nassaj, H. Sarpoolaky, J. Alloys Compd. 456 (2008) 282–285.
[15] S.A. Hassanzadeh-Tabrizi, E. Taheri-Nassaj, J. Am. Ceram. Soc. 91 (2008) 3546–3551.
[16] D. Sarkar, S. Adak, N.K. Mitra, Compos. Part A 38 (2007) 124–131.
[17] M. Shojaie-Bahaabad, E. Taheri-Nassaj, Mater. Lett. 62 (2008) 3364–3366.
[18] W.F.M. Groot Zevert, A.J.A. Winnubst, G.S.A.M. Theunissen, A.J. Burggraaf, J. Mater. Sci. 25 (1990) 3449–3455.
[19] A.A. Bukaemskiy, D. Barrier, G. Modolo, J. Eur. Ceram. Soc. 29 (2009) 1947–1954.
[20] M. Mayo, Int. Mater. Rev. 41 (1996) 85–115.
[21] H. Duong, J. Wolfenstine, Mater. Sci. Eng. A172 (1993) 173–179.
[22] K. Niihara, J. Ceram. Soc. Japan 99 (1991) 974–982.